II International Conference on Particle-based Methods - Fundamentals and Applications
PARTICLES 2011
E. Oñate and D.R.J. Owen (Eds)

MULTIBODY CONTACT DYNAMICS WITH COROTATIONAL FINITE ELEMENTS AND ROUGH BACKGROUND MESH

TOMASZ KOZIARA, ŁUKASZ KACZMARCZYK AND NENAD BIĆANIĆ

School of Engineering
University of Glasgow, Glasgow G12 8LT, UK
e-mail: t.koziara@civil.gla.ac.uk

Key words: co-rotational, FEM, simplified deformations, Contact Dynamics

Abstract. In this work we demonstrate a simple kinematic model allowing for a variable amount of deformability for arbitrary shapes. A co-rotational finite element formulation is integrated over a shape submerged in a rough background mesh. The presented formulation allows to approximate the structural length-scale shock waves within a multi-body structure, which might be seen as a refinement of the solely rigid approach, for which such resolution is not readily available. For best illustration of core ideas, only simple one-body examples are given in the current paper. Nevertheless, the kinematic model has been employed within the Contact Dynamics time-stepping method and applied to large scale, parallel simulations of blocky structures with contact and friction. The source code is available at http://solfec.googlecode.com.

1 INTRODUCTION

Rigid kinematics is commonly used in industrial multibody simulations (e.g. robotics or granular flow). This level of kinematic description is often sufficient when dynamic effects corresponding to the collective deformable behavior of bodies can be neglected. Whenever this is not the case though, a modeler often runs into problems with the computational bottleneck of processing many interacting bodies, discretised with fine Finite Element meshes. Because in the classical formulation mesh and shape coincide, small features of the shape may result in the necessity of resolving deformation length scales that might not be of practical interest in the overall collective behavior of large multibody problems. In order to facilitate this level of modeling, a simple extension of the classical Finite Element approach has been implemented in Solfec [5]: shapes and FE meshes can be prescribed independently. This is pictured in Figure 1, where a geometrical model of a complex shape is contained inside of background FE mesh with 96 nodes. In a multibody model of

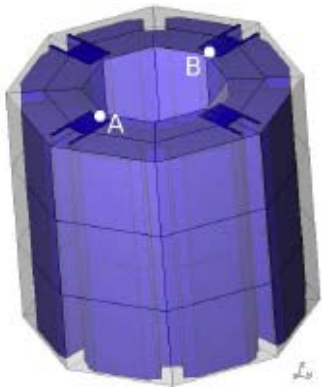

Figure 1: An example of a complex shape, whose deformable kinematics is approximated by a nonconforming background mesh with 288 degrees of freedom.

a practical interest many thousands of such bodies interact through contact and friction. Clearly, it would be computationally difficult to resolve this kind of collective geometry by means of a fine, matching FE mesh.

Using the background mesh is only a simple, technical idea. The core contribution of this paper is the co-rotational Finite Element formulation, which allows to apply deformability at a very low cost. We adapt the work of Kaczmarczyk et al. [4] and design a simple body-wise co-rotational formulation, for which the global stiffness matrix is assembled and inverted only once. The subsequent linear solves only reuse a once computed factorization, while still being able to correctly account for large rigid rotations. Our approach is well suited for stiff, deformable bodies whose gross rigid motion is of engineering interest and whose deformability plays some role in a collective multibody dynamics. To this end we use stiffness-proportional damping, which does not affect the rigid motion, but which allows to model a range of post-impact behavior in an energy consistent, dissipative manner. Modeling multiple impacts and shock waves within a solely rigid, implicit multibody formulation is not possible in general, hence our approach provides a relatively inexpensive refinement in this respect.

2 ROTATED DYNAMICS

Consider a stiff body capable of large rigid motion and small elastic deformations. We can parametrize its motion as

$$\mathbf{x}\left(\mathbf{X},t\right)=\mathbf{X}+\mathbf{S}\left(\mathbf{X}\right)\mathbf{q}\left(t\right) \tag{1}$$

where $\mathbf{x}$ is a spatial point, $\mathbf{X}$ is a referential point, t is time, $\mathbf{S}$ stores finite element shape functions, and $\mathbf{q}$ stores nodal displacements. Because we consider infinitesimal deformations about a possibly translated and rotated shape, it makes sense to talk about the gross rigid motion

$$\mathbf{x}_r\left(\mathbf{X},t\right)=\mathbf{\Lambda}\left(t\right)\left(\mathbf{X}-\mathbf{A}\right)+\mathbf{a}\left(t\right) \tag{2}$$

where $\mathbf{\Lambda}$ is a rotation operator, $\mathbf{A}$ is a referential point, and $\mathbf{a}$ is a spatial image of $\mathbf{A}$. These two motions differ by the amount of deformation

$$\mathbf{d}\left(\mathbf{X},t\right)=\mathbf{x}\left(\mathbf{X},t\right)-\mathbf{x}_r\left(\mathbf{X},t\right) \tag{3}$$

Assuming that $\mathbf{Z}_i$ are coordinates of mesh nodes, we can collect $\mathbf{d}\left(\mathbf{Z}_i,t\right)$ into a vector

$$\mathbf{d}=\left[\begin{array}{c}\ldots\\ \mathbf{Z}_i+\mathbf{q}_i-\mathbf{\Lambda}\left(\mathbf{Z}_i-\mathbf{A}\right)-\mathbf{a}\\ \ldots\end{array}\right] \tag{4}$$

where $\mathbf{q}_i$ represent displacements at node i. We can also express $\mathbf{d}$ from the perspective of the reference configuration

$$\mathbf{d}_0=\underline{\mathbf{\Lambda}}^T\mathbf{d} \tag{5}$$

where $\underline{\mathbf{\Lambda}}$ denotes a block-diagonal square matrix composed of $\mathbf{\Lambda}$ and matching the dimension of $\mathbf{d}$. We can then write down a discrete form of momentum conservation

$$\mathbf{M}d\mathbf{u}+\underline{\mathbf{\Lambda}}\mathbf{K}\underline{\mathbf{\Lambda}}^T\left(\mathbf{d}dt+\eta\mathbf{u}dt\right)=\mathbf{f}dt \tag{6}$$

where $\mathbf{M}$ is a mass matrix, $d\mathbf{u}$ and dt are suitable velocity and time measures, $\mathbf{K}$ is an initial stiffness matrix $\mathbf{K}=\partial^2\Psi/\partial\mathbf{q}\partial\mathbf{q}$ at $t=0$ where Ψ is a hyper-elastic potential, and $\mathbf{f}$ is an external force. We note, that the term $\eta\underline{\mathbf{\Lambda}}\mathbf{K}\underline{\mathbf{\Lambda}}^T\mathbf{u}$ corresponds to a stiffness-proportional damping, which can be used to damp out fast elastic oscillations without affecting the rigid body motion. At this point it is useful to notice that $\mathbf{A}$ and $\mathbf{a}$ in (4) play no role in (6) since rigid translations correspond to zero eigenvalues of $\mathbf{K}$. Hence, we can redefine $\mathbf{d}$ as

$$\mathbf{d}=\left[\begin{array}{c}\ldots\\ \left(\mathbf{I}-\mathbf{\Lambda}\right)\mathbf{Z}_i+\mathbf{q}_i\\ \ldots\end{array}\right]=\left(\underline{\mathbf{I}-\mathbf{\Lambda}}\right)\mathbf{Z}+\mathbf{q} \tag{7}$$

where $\mathbf{I}$ is the 3×3 identity. This corresponds to the deformation

$$\mathbf{d}\left(\mathbf{X},t\right)=\mathbf{x}\left(\mathbf{X},t\right)-\mathbf{\Lambda}\left(t\right)\mathbf{X} \tag{8}$$

which superposes rigid translation and small deformations of the body. As a result symmetric part of gradient of (8) equals to the symmetric part of the gradient of (3). This fact will be used in Section 4.

3 TIME INTEGRATION

Consider a multi-body domain with constraints. Let the constraint reactions be denoted by $\mathbf{R}$ and the relative constraints velocities be denoted by $\mathbf{U}$. Let also the constraints equations be denoted by $\mathbf{C}(\mathbf{U}, \mathbf{R}) = \mathbf{0}$. When talking about $\mathbf{q}$, $\mathbf{u}$, $\mathbf{\Lambda}$, etc. we now mean suitable collections of per-body entities. In order to integrate in time, a half-step configuration is extrapolated first

$$\mathbf{q}^{t+h/2} = \mathbf{q}^t + \frac{h}{2}\mathbf{u}^t \tag{9}$$

$$\mathbf{\Lambda}_1 = \hat{\mathbf{\Lambda}}\left(\mathbf{q}^{t+h/2}, \mathbf{\Lambda}^t\right). \tag{10}$$

A global $\mathbf{u}$ to local $\mathbf{U}$ velocity transformation operator is computed next

$$\mathbf{H} = \mathbf{H}\left(\mathbf{q}^{t+h/2}\right) \tag{11}$$

where for example, in case of Finite Elements, $\mathbf{H}$ is a global to local coordinates transformation of the shape functions values nonzero at constraint points. The number of rows of $\mathbf{H}$ depends on the number of constraints, while its rank is related to their linear independence. The momentum balance

$$\mathbf{b} = \mathbf{M}\mathbf{u}^t + h\mathbf{f}^{t+h/2} - h\underline{\mathbf{\Lambda}_1}\mathbf{K}\underline{\mathbf{\Lambda}_1}^T\left[\left(\underline{\mathbf{I} - \mathbf{\Lambda}_1}\right)\mathbf{Z} + \mathbf{q}^{t+h/2} + \eta\mathbf{u}^t\right] \tag{12}$$

$$\left(\mathbf{M} + \frac{h^2}{4}\underline{\mathbf{\Lambda}_1}\mathbf{K}\underline{\mathbf{\Lambda}_1}^T\right)\mathbf{u}^{t+h} = \mathbf{b} + \mathbf{H}^T\mathbf{R} \tag{13}$$

together with the transformation

$$\mathbf{U} = \mathbf{H}\mathbf{u}^{t+h} \tag{14}$$

and the constraints equations

$$\mathbf{C}(\mathbf{U}, \mathbf{R}) = \mathbf{0} \tag{15}$$

are used to evaluate the velocity $\mathbf{u}^{t+h}$ and the constraint reactions $\mathbf{R}$. This is further commented on in Section 5. For the sake of simplicity the term $\eta\mathbf{u}^t$ is explicit in (12). The stiffness-proportional damping is a pragmatic, numerical device here: we use to avoid uninteresting oscillations and to drive post-impact behavior. Finally, the end-step configuration is updated

$$\mathbf{q}^{t+h} = \mathbf{q}^{t+h/2} + \frac{h}{2}\mathbf{u}^{t+h} \tag{16}$$

$$\mathbf{\Lambda}^{t+h} = \hat{\mathbf{\Lambda}}\left(\mathbf{q}^{t+h}, \mathbf{\Lambda}_1\right). \tag{17}$$

The above scheme is linearly-implicit: as far as unconstrained motion is concerned only one linear system needs to be solved per time step. A fully implicit version of the time integration scheme will be presented in a longer version of the article.

4 UPDATING ROTATION

Kaczmarczyk et al. [4] developed a convenient way of updating rotation, as needed in (10), and (17). Because the antisymmetric part of the gradient of the deformational displacement (8) corresponds to an infinitesimal rotation at a point, an average of it

$$\overline{\nabla \mathbf{d}} = \frac{1}{V} \int_{\Omega} \nabla \mathbf{d} \left(\mathbf{X}, t \right) - \nabla \mathbf{d}^T \left(\mathbf{X}, t \right) d\Omega \tag{18}$$

represents the resultant infinitesimal rotation of the body (V is the volume). For every $\mathbf{d}$, $\mathbf{\Lambda}$ is incremented in such a way so to minimise $\overline{\nabla \mathbf{d}}$. The divergence theorem is exploited in [4] in order to obtain

$$\mathrm{vec} \left[\int_{\Omega} \nabla \mathbf{d} - \nabla \mathbf{d}^T d\Omega \right] = \int_{\Gamma} \mathbf{n} \times \mathbf{d} d\Gamma \tag{19}$$

where vec$[\cdot]$ makes a pseudo-vector out of an antisymmetric matrix, and $\mathbf{n}$ is the spatial outward normal to the surface of the body. The surface integral can be further resolved

$$\begin{aligned} \mathbf{h} &= \int_{\Gamma} \mathbf{n} \times \mathbf{d} d\Gamma = \int_{\Gamma} \mathrm{skew} \left[\mathbf{n} \right] \mathbf{d} d\Gamma \\ &= \int_{\Gamma} \mathrm{skew} \left[\mathbf{\Lambda N} \right] \mathbf{d} d\Gamma = \int_{\Gamma} \mathrm{skew} \left[\mathbf{N} \right] \mathbf{\Lambda}^T \mathbf{d} d\Gamma \\ &= \int_{\Gamma} \mathrm{skew} \left[\mathbf{N} \right] \mathbf{\Lambda}^T \left[\mathbf{X} + \mathbf{S} \left(\mathbf{X} \right) \mathbf{q} - \mathbf{\Lambda X} \right] d\Gamma \\ &= \int_{\Gamma} \mathrm{skew} \left[\mathbf{N} \right] \mathbf{\Lambda}^T \mathbf{x} d\Gamma \end{aligned} \tag{20}$$

where the simplification to the last line follows from the assumption $\int_{\Gamma} f d\Gamma \simeq \int_{\Gamma_0} f d\Gamma_0$ and the fact that $\int_{\Gamma} \mathrm{skew} \left[\mathbf{N} \right] \mathbf{X} d\Gamma = \mathrm{vec} \left[\int_{\Omega} \nabla \mathbf{X} - \nabla \mathbf{X}^T d\Omega \right] = \mathbf{0}$. The operator skew $[\cdot]$ makes a skew symmetric matrix out of a vector so that $\mathrm{skew} \left[\mathbf{n} \right] \mathbf{d} = \mathbf{n} \times \mathbf{d}$. The following functional is then defined

$$\mathbf{J} \left(\mathbf{q}, \mathbf{\Lambda} \right) = \frac{1}{2} \mathbf{h}^T \left(\mathbf{q}, \mathbf{\Lambda} \right) \mathbf{h} \left(\mathbf{q}, \mathbf{\Lambda} \right) \tag{21}$$

and the $\hat{\mathbf{\Lambda}}$ mapping employed in the previous section takes form

$$\hat{\mathbf{\Lambda}} \left(\mathbf{q}, \mathbf{\Lambda} \right) = \exp \left(\mathbf{\Phi} \right) \mathbf{\Lambda}, \text{ where } \mathbf{\Phi} = \arg\min \mathbf{J} \left(\mathbf{q}, \exp \left(\mathbf{\Phi} \right) \mathbf{\Lambda} \right) \tag{22}$$

where $\exp[\cdot]$ is the exponential map. Gauss-Newton iterations are exploited in order to compute the minimiser

$$\mathbf{\Phi}^{i+1} = \mathbf{\Phi}^i - \left\{\partial^2 \mathbf{J}/\partial\mathbf{\Phi}\partial\mathbf{\Phi}\right\}^{-1} \left\{\partial \mathbf{J}/\partial\mathbf{\Phi}\right\} \tag{23}$$

where

$$\begin{aligned} \partial \mathbf{J}/\partial\mathbf{\Phi} &= \mathbf{h}^T \left[\partial \mathbf{h}/\partial\mathbf{\Phi}\right] \\ &= \mathbf{h}^T \left[\int_\Gamma \text{skew}\left[\mathbf{N}\right] \mathbf{\Lambda}^T \frac{\partial \exp\left(-\mathbf{\Phi}\right)}{\partial\mathbf{\Phi}} \mathbf{x} d\Gamma\right] \end{aligned} \tag{24}$$

$$\begin{aligned} \partial^2 \mathbf{J}/\partial\mathbf{\Phi}\partial\mathbf{\Phi} &= \left[\partial \mathbf{h}/\partial\mathbf{\Phi}\right]^T \left[\partial \mathbf{h}/\partial\mathbf{\Phi}\right] + \mathbf{h}^T \left[\partial^2 \mathbf{h}/\partial\mathbf{\Phi}\partial\mathbf{\Phi}\right] \\ &\simeq \left[\partial \mathbf{h}/\partial\mathbf{\Phi}\right]^T \left[\partial \mathbf{h}/\partial\mathbf{\Phi}\right] + \delta \mathbf{I} \end{aligned} \tag{25}$$

and δ is large enough to make $\partial^2 \mathbf{J}/\partial\mathbf{\Phi}\partial\mathbf{\Phi}$ positive definite, ensuring a descent direction in (23). In practice, for this 3×3 problem, $\delta = 0$ works well.

5 HANDLING CONSTRAINTS

Let

$$\mathbf{A} = \mathbf{M} + \frac{h^2}{4} \underline{\mathbf{\Lambda}_1} \mathbf{K} \underline{\mathbf{\Lambda}_1}^T. \tag{26}$$

In order to compute the constraints reactions we need to solve the nonlinear system

$$\mathbf{A}\mathbf{u}^{t+h} = \mathbf{b} + \mathbf{H}^T \mathbf{R} \tag{27}$$

$$\mathbf{U} = \mathbf{H}\mathbf{u}^{t+h} \tag{28}$$

$$\mathbf{C}\left(\mathbf{U}, \mathbf{R}\right) = \mathbf{0}. \tag{29}$$

An important aspect in this context is inversion of $\mathbf{A}$. For a diagonal (lumped) $\mathbf{M}$ (with constant per-node values) there holds

$$\mathbf{A} = \underline{\mathbf{\Lambda}_1} \left[\mathbf{M} + \frac{h^2}{4} \mathbf{K}\right] \underline{\mathbf{\Lambda}_1}^T = \underline{\mathbf{\Lambda}_1} \mathbf{A}_0 \underline{\mathbf{\Lambda}_1}^T \tag{30}$$

and it follows

$$\mathbf{A}^{-1} = \left[\underline{\mathbf{\Lambda}_1} \mathbf{A}_0 \underline{\mathbf{\Lambda}_1}^T\right]^{-1} = \underline{\mathbf{\Lambda}_1} \left[\underline{\mathbf{\Lambda}_1} \mathbf{A}_0\right]^{-1} = \underline{\mathbf{\Lambda}_1} \mathbf{A}_0^{-1} \underline{\mathbf{\Lambda}_1}^T \tag{31}$$

so that it is enough to invert $\mathbf{A}_0$ only once.

A variety of constraints can be described in the form (29). These include contact, friction and a range of common equality constraints. An example of solving the system (27-29) in case of frictional contact constraints can be found in [3, 5], while a broader overview can be found in [2, 1].

6 ROUGH BACKGROUND MESH

A geometrical model of a complex shape, contained inside of background FE mesh with 96 nodes is presented in Figure 1. The technicalities of the background mesh approach are quite straightforward. The background mesh needs to properly contain the modeled shape. Since the Finite Element shape functions are partition of unity regardless of whether the mesh matches the shape or not, the overall convergence properties of FEM are not affected. There are three practical aspects of the implementation:

1. Space integration. We represent shapes as juxtapositions of arbitrary convex polyhedrons. We then compute a set theoretic intersection of these polyhedrons with FE mesh elements. This results in a set of *pieces*: convex polyhedrons resulting from volumetric intersections of the input polyhedrons and FE elements. For each element we create a list of pieces contained inside of it. Whenever volumetric integration needs to be done (e.g. to compute internal forces or stiffness/mass matrix) we integrate over these pieces, using the FE shape functions of the background mesh.

2. Boundary conditions. In our code [5] boundary conditions are prescribed my means of Lagrange multipliers. There is then no general difficulty with prescribing boundary conditions in this particular context. Contact detection and resulting contact constraints are based on the actual body shape. The resulting kinematic and dynamic derivations correspond to the background FE mesh, just as they would in the conventional sense.

3. Inertia properties. If a consistent mass matrix is used, the shape of the background mesh and the actual shape of a body do not need to be well aligned. When a lumped mass is used though, the background FE mesh should tightly approximate the actual shape. This is natural, since some of the information is lost in the process of lumping the mass properties. In our applications we use row-summed lumped mass and thus background meshes are usually tight.

7 EXAMPLES

The examples below are not aimed at demonstration of accurate predictions of small deformations of analysed bodies. Instead, we demonstrate that the dominant rigid motion can be well reproduced by means of the co-rotational formulation, while the deformability combined with the stiffness-proportional damping can be used to model post-impact

behavior. The practicality of such approach will yet need to be validated. Here, we only indicate its potential usefulness.

7.1 Free rotation of a body[1]

In this example we rotate the body from Figure 1. Elastic material parameters are 1E10, 0.2, 2E3 for respectively the Young modulus, Poisson ratio and mass density. The initial angular velocity of value 2π is prescribed along the longitudinal direction. For this input the body makes one full rotation per one second of simulation.

We symmetrically pick two opposite points aligned with the x direction at the internal cylindrical surface of the body (points A and B in Figure 1). The inner radius of the body is 0.1315 so that their initial distance $|\mathbf{A} - \mathbf{B}| = 0.263$. We picture this distance as function of time, which allows to show radial expansion of the body due to centrifugal effects. We also monitor the y displacement of one of the picked points and compare it with a corresponding y displacement of a rigid body model of the same problem. This way we can see whether the FE model is in phase with the gross rigid motion of the body.

The first goal of this example is to test how stable the co-rotational integration scheme is. Without damping, $\eta = 0$, and for a too large time step the extrapolated estimate of the half-step rotation in (10) will gradually diverge from the actual rotation of the body. This will cause excessive internal forces due to erroneous interpretation of deformational displacements in (12). Eventually this will lead to uncontrolled swelling of the body. In Figure 2 (left) an onset of this sort of behaviour can be observed in for time step 0.005, corresponding to 1.8 deg of incremental rotation per time step. Clearly, for too large time steps, undamped co-rotational scheme will produce poor results. The problem with stability can be fixed by including a small amount of stiffness-proportional damping, $\eta =$ 1E-3. This is illustrated in Figure 2 (right), where the y displacements of point A are compared over 10 seconds of simulation for the FE and rigid bodies. The agreement between both models is very good.

In Figure 3 the time history of the inner diameter $|\mathbf{A} - \mathbf{B}|$ is plotted for the time step 0.001 and the damping parameter $\eta \in \{0, \text{1E-5}, \text{1E-4}\}$. The diameter stably oscillates for the undamped case. For damped runs the diameter comes to a steady state with its value dependent on the damping parameter. The larger the damping parameter, the larger the stabilized diameter. This corresponds to the fact that the outward radial component of the velocity contributes an artificial external force through the stiffness-proportional damping. Nevertheless, the amount of deformation due to this effect remains far below values of engineering interest.

Finally, Table 1 compares time integration runtimes for one second runs with time step 0.001, computed for rigid (6 degrees of freedom), co-rotational FE and Total Lagrangian FE models (288 degrees of freedom). The co-rotational formulation is about 16 times faster than the Total Lagrangian one. This ratio will increase for larger meshes.

[1]Input file at: http://code.google.com/p/solfec/source/browse/inp/body-rotate.py

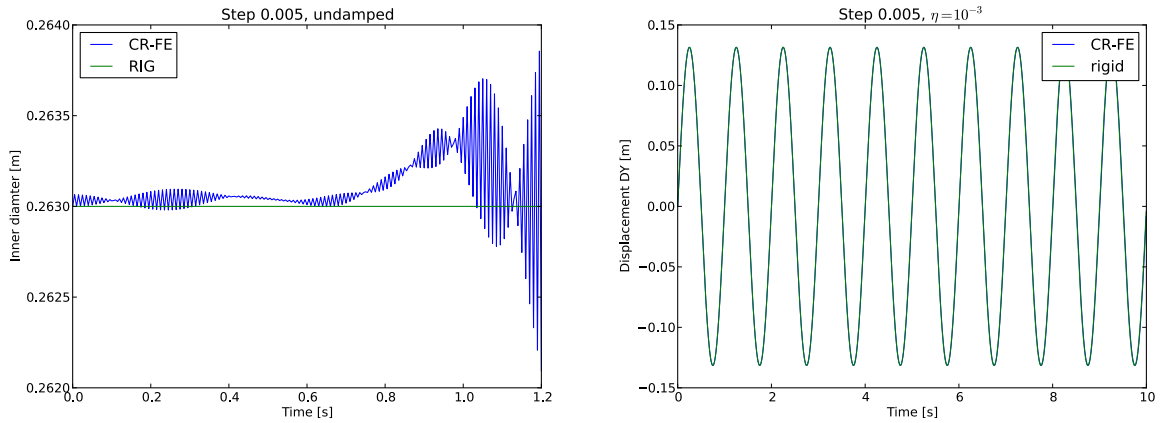

Figure 2: Body rotation, time step 0.005. Left: unstable, undamped run; time history of the inner diameter of the body. Right: stable, damped run (η = 1E-3); time history of the y displacement of point A in Figure 1; FE and rigid motion histories overlap.

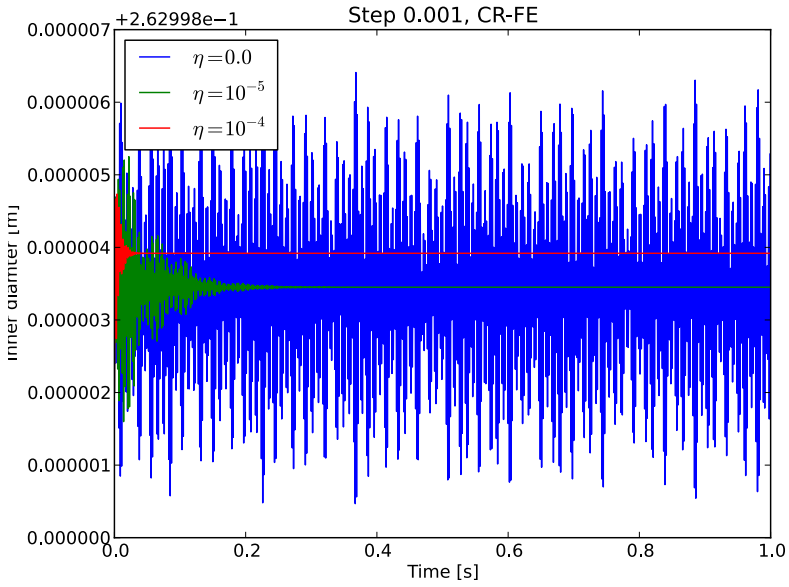

Figure 3: Body rotation, time step 0.001. Time history of $|\mathbf{A}-\mathbf{B}|$ for stable runs with and without damping, $\eta \in \{0, 1\text{E-}5, 1\text{E-}4\}$.

rigid	CR-FE	TL-FE
0.14	8.56	137

Table 1: Body rotation. Comparison of time integration runtimes for rigid, co-rotational FE and Total Lagrangian FE formulations. One second run with time step 0.001.

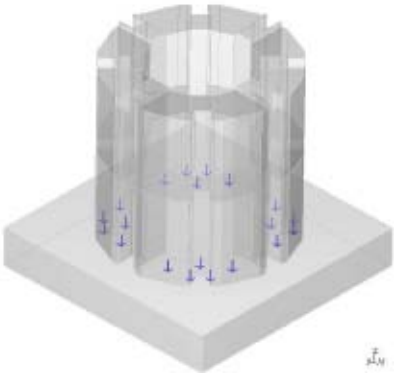

Figure 4: Body impact. Twenty contact points between the body and the obstacle.

7.2 Flat impact of a body [2]

In this example we vertically drop the body from Figure 1 onto a flat rigid obstacle. The material parameters are like in the previous example. We assume zero friction and use the velocity level Signorini impact model

$$U_N \geq 0, \;\; R_N \geq 0, \;\; U_N R_N = 0 \tag{32}$$

where U_N is the normal relative velocity between the body and the obstacle, and R_N is the normal impulsive force between the two objects. At the contact point level this corresponds to an ideally plastic impact: a point mass remains on the obstacle after hitting it. Similarly for a rigid body model this means that after hitting the obstacle the body will remain there, without rebound. If the body is deformable though, it will undergo a complex pattern of local and global deformations that will store and subsequently release some energy, resulting in a degree of rebound. This is a complex phenomenon, whose accurate modeling requires a fine discretization in order to capture inelastic effects near the impact zone and elastic stress waves that are excited and subsequently damped within the bulk of the body. This we cannot afford in a structure comprising thousands of bodies. The aim of this exercise is to see whether some post-impact behavior can be modelled given the relatively large space and time resolution that is available to us.

In this example the body is placed 1 meter above the flat rigid obstacle and it falls freely under gravity $(0, 0, -10)$. When it hits the obstacle its vertical velocity is about -4.45 m/s. Due to the way the geometry is modeled, 20 contact points are created upon first impact, cf. Figure 4, and the inequality constraint (32) is implicitly enforced at all of them. The post-impact behavior of the body corresponds then to the interplay of the immediate loss of energy at contact points due to the ideally plastic character of the impact law (32), and to the dissipation of the energy in the bulk of the body due to the stiffness-proportional damping.

[2]Input file at: http://code.google.com/p/solfec/source/browse/inp/body-impact.py

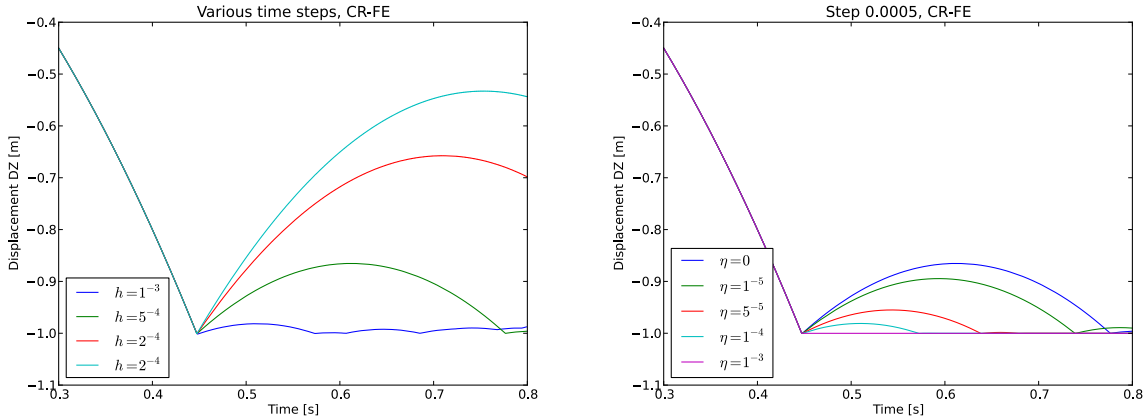

Figure 5: Body impact. The z displacement histories of point **A**. Left: undamped run for time steps $h \in \{1E\text{-}4, 2E\text{-}4, 5E\text{-}4, 1E\text{-}3\}$. Right: damped runs for $\eta \in \{0, 1E\text{-}5, 5E\text{-}5, 1E\text{-}4, 1E\text{-}3\}$.

The stable explicit time step for this example is about of 2E-5. Integrating in time with this step allows to account for all deformation modes and hence store a maximal possible amount of energy during impact. When using an implicit time integration we choose to skip some of the higher frequency modes in order to save computational time. As a consequence we operate on a subset of the modes and, with increasing step size, we gradually store less and less energy in deformations. This can bee seen in Figure 5 (left), where the post-impact behavior of undamped runs becomes increasingly more rigid for larger time steps. In the same figure on the right we can see the time history of the z displacement of point **A** for step 0.0005 and for a range of damping values. Clearly, we are able to reproduce post-impact behavior ranging from partially elastic to ideally plastic.

8 CONCLUSIONS

We have presented a computationally modest way of accounting for large rotations in the context of stiff deformable kinematics. Our time integration scheme, combined with the contact constraint (32) results in energetically consistent, dissipative scheme (also in case of friction). The degree of deformability and the time resolution can be freely adjusted depending on the available computer power or modelling needs, while the stiffness-proportional damping allows to independently obtain a range of post-impact behavior (without affecting the rigid motion). This seems particularly attractive in the context of multibody problems for which deformability of individual bodies contributes to a collective behavior. Of course, the greatest challenge and the matter of future work is to validate this approach on available experimental data. In the meantime, we would like to invite the readers to test our approach by downloading Solfec from http://code.google.com/p/solfec/.

ACKNOWLEDGEMENTS

The support from EDF Energy is gratefully acknowledged.

References

[1] V. Acary and B. Brogliato. *Numerical Methods for Nonsmooth Dynamical Systems*, volume 35 of *Lecture Notes in Applied Lecture Notes in Applied and Computational Mechanics*. Springer Verlang, 2008.

[2] Bernard Brogliato. *Nonsmooth Mechanics*. Communications and Control Engineering. Springer Verlang, 1999.

[3] M. Jean. The non-smooth contact dynamics method. *Computer Methods in Applied Mechanics and Engineering*, 177(3-4):235–257, 1999.

[4] Lukasz Kaczmarczyk, Tomasz Koziara, and Chris J. Pearce. Corotational formulation for 3d solids: an analysis of geometricaly nonlinear foam deformation. *In preparation*, 2011.

[5] Tomasz Koziara and Nenad Bićanić. A distributed memory parallel multibody contact dynamics code. *International Journal for Numerical Methods in Engineering*, 2011.